MiLDEdit: Reasoning-Based Multi-Layer Design Document Editing

Anonymous authors
Paper under double-blind review

Figure 1: Our benchmark MiLDEBench is the first targeting to transparent-background, multi-layer design document editing.

Abstract

Real-world *design documents* (e.g., posters) are inherently multi-layered, combining decoration, text, and images. Editing them from natural-language instructions requires fine-grained, layer-aware reasoning to identify relevant layers and coordinate modifications. Prior work largely overlooks *multi-layer design document editing*, focusing instead on single-layer image editing or multi-layer generation, which assume a flat canvas and lack the reasoning needed to determine *what* and *where* to modify. To address this gap, we introduce the Multi-Layer Document Editing Agent (**MiLDEAgent**), a reasoning-based framework that combines an RL-trained multimodal reasoner for layer-wise understanding with an image editor for targeted modifications. To systematically benchmark this setting, we introduce the Multi-Layer Document Editing Benchmark (**MiLDEBench**), a human-in-the-loop corpus of over 20K design documents paired with diverse editing instructions. The benchmark is complemented by a task-specific evaluation protocol, **MiLDEEval**, which spans four dimensions including instruction following, layout consistency, aesthetics, and text rendering. Extensive experiments on 13 open-source and 2 closed-source models reveal that existing approaches fail to generalize: open-source models often cannot complete multi-layer document editing tasks, while closed-source models suffer from format violations. In contrast, MiLDEAgent achieves strong layer-aware reasoning and precise editing, significantly outperforming all open-source baselines and attaining performance comparable to closed-source models, thereby establishing the first strong baseline for multi-layer document editing.

1 Introduction

While recent breakthroughs in image generation have transformed creative workflows, editing real-world design documents such as posters, flyers, and slides still remains an open challenge. Unlike natural images, these design documents are intrinsically multi-layered, combining backgrounds, graphics, text, and foreground imagery in a carefully structured hierarchy. Effective editing requires reasoning about which layers are relevant to user intent, how their relationships constrain possible modifications, and where changes can be applied without disrupting layout or occluding critical content. Existing reasoning-based editing methods (Jiang et al., 2025; Chen et al., 2025b; Zhang et al., 2025b) are built for flat, single-layer canvases and fail to capture this complexity. Besides, despite some works focuing on design document generation (Huang et al., 2024; Pu et al., 2025; Chen et al., 2025a), layer-aware document editing remains unexplored, leaving a critical gap in vision-language reasoning and multimodal editing.

To fill this gap, we propose the first benchmark for reasoning-based *multi-layer* document editing, Multi-Layer Document Editing Benchmark (**MiLDEBench**). MiLDEBench systematically focuses on *content editing*, which entails semantically coherent modifications while maintaining the visual and structural integrity of the document. Building upon 20K transparent-background templates from the public Crello dataset (Yamaguchi, 2021), we synthesize 50K natural-language editing instructions and 87K layer-aligned edit steps via a hybrid generation pipeline that integrates open-source multimodal LLMs with human-in-the-loop verification. To approximate real-world application scenarios where users come from diverse backgrounds, we design persona-conditioned and document-conditioned prompts that capture heterogeneous editing intents, ensuring that the dataset reflects a broad spectrum of user needs (*e.g.*, converting a Christmas card into a Halloween card).

To evaluate this task, we introduce **MiLDEEval**, a task-specific protocol encompassing four core dimensions: *instruction following*, *layout consistency*, *aesthetics*, and *text rendering*. These dimensions establish a standardized testbed for reasoning-intensive, layer-aware editing that mirrors real-world design scenarios. To better align with human perception, we aggregate these criteria into a unified metric, **MiLDEScore**. This composite score provides a holistic quality assessment and demonstrates a stronger correlation with human preference than previous protocols or individual metrics. We benchmark 13 open-source and 2 closed-source models on MiLDEBench. Given that most existing models produce only flat outputs, we adopt a single-round editing setting where models generate one edited poster from a document and instruction without explicit layer access. Even in this simplified setting, open-source models show limited instruction following, while closed-source models often sacrifice layout consistency for semantic alignment. Notably, incorporating explicit reasoning yields only modest gains, suggesting that current text-centric reasoning fails to leverage multi-layer structures. These findings confirm that design document editing exceeds current paradigms, motivating a specialized reasoning-based, layer-aware approach.

To address these gaps, we propose **MiLDEAgent**, a reasoning-based, layer-aware editing agent. MiLDEAgent integrates (i) an RL-trained multimodal reasoner, optimized via a novel reward function for layer identification and prompt synthesis, and (ii) a modular editor for targeted, layer-specific modifications. Experimental results show that explicit layer-awareness is crucial for controllable editing. MiLDEAgent surpasses open-source baselines by 82.78% in MiLDEScore, achieves performance comparable to closed-source models, and superior layout consistency. By reaching the best balance between *instruction adherence* and *structural fidelity*, MiLDEAgent underscores the efficacy of reasoning-based multi-layer editing.

We summarize our main contribution as follows:

- **Task and Benchmark.** We formalize the problem of *multi-layer design document editing* and introduce **MiLDEBench**, a corpus of 20K documents with 50K editing instructions and 87K layer-aligned steps, along with the task-specific evaluation protocol **MiLDEEval** and **MiLDEScore**.
- **Comprehensive Evaluation.** We benchmark 13 open-source and 2 closed-source systems, identifying consistent challenges in instruction following, layout fidelity, and coordination across layers.
- **Method and Results.** We propose **MiLDEAgent**, which combines a GRPO-trained multimodal reasoner with a pluggable layer-wise editor. MiLDEAgent demonstrates strong instruction adherence and layout consistency, surpassing open-source baselines and performing competitively with closed-source systems.

2 Related Work

2.1 Multi-layer Transparent Image Generation

Prior research on multi-layer design documents has primarily focused on generation and decomposition. Early efforts centered on dataset construction, either by extracting layers from natural image corpora (e.g., LAION (Schuhmann et al., 2022), COCO (Lin et al., 2014)) (Zhang et al., 2023b; Huang et al., 2024; Tudosiu et al., 2024; Gu et al., 2024) or curating professional graphic designs (Yamaguchi, 2021; Pu et al., 2025). Based on these, recent models have advanced multi-layer reasoning (Deng et al., 2025; Xiao et al., 2025b), synthetic supervision pipelines (Burgert et al., 2024; Chen et al., 2025a), and coordinated generation with semantic dependencies (Huang et al., 2024; Pu et al., 2025). Another dimension is layout-related research work that focuses on editing layout (Suri et al., 2024; Avudaiappan & Murali, 2025), decomposing (Nie et al., 2025; Suzuki et al., 2025) or generating layout document or images Feng et al. (2023); Bar-Tal et al. (2022). Our work is different from theirs in that it focuses on reasoning-based, multi-layer transparent image editing.

More recently, research has shifted toward editability via image-to-layer decomposition (e.g., Qwen-Image-Layered (Yin et al., 2025)), enabling post-hoc manual edits. However, these methods primarily focus on layer discovery or reconstruction from flat images, rather than instruction-driven modification of existing design documents. In contrast, real-world workflows require iterative, high-level editing while maintaining structural consistency—a need largely unmet by prior generation-centric work. To bridge this gap, we introduce **MiLDEBench**, the first benchmark pairing layered documents with document-level instructions and human-validated edit traces, shifting the focus to faithful and controllable multi-layer editing.

2.2 Reasoning-based Image Generation & Editing

Driven by recent advances in large language models (LLMs) and training algorithms (Shao et al., 2024; Yu et al., 2025b), reasoning-oriented image generation and editing have achieved remarkable progress (Zhang et al., 2025b; Duan et al., 2025; Jiang et al., 2025; Wu et al., 2025b; Guo et al., 2025; Pan et al., 2025; Jin et al., 2024; Zhang et al., 2025a). Current methods may be classified according to the manner in which reasoning is incorporated into the pipeline: (i) *prompt interpretation*, where the system resolves compositional or implicit semantics in user instructions (*e.g.*, temporal or causal cues) prior to editing (Chen et al., 2025b; Sun et al., 2025; Jin et al., 2024; Zhang et al., 2025a); (ii) *prompt extension*, which augments concise instructions with additional structure (*e.g.*, constraints, spatial hints) to enhance output faithfulness (Wu et al., 2025b; Jiang et al., 2025; Zhang et al., 2025b; Duan et al., 2025); and (iii) *generation-time reasoning*, which introduces self-checking or iterative refinement during synthesis to enforce consistency with requirements (Guo et al., 2025; Pan et al., 2025). Nevertheless, these approaches are predominantly built on the assumption of a single, flattened canvas and thus lack *layer-aware* reasoning about hierarchical structure, inter-layer dependencies, and document-level constraints (*e.g.*, text fidelity, non-occluding layout). As a result, even when instructions are correctly interpreted, edits often fail to account for relevant layers or disrupt spatial organization. We introduce **MiLDEAgent**, which formalizes *multi-layer document editing* as a reasoning task and ensures consistency via layer selection, layer-wise editing instruction generation, and layer editing.

3 MiLDEBench

3.1 Preliminaries

We define multi-layer document editing as a two-stage process consisting of reasoning and editing. A document D is represented as an ordered set of transparent layers $\mathcal{L} = \{L_i \in \mathbb{R}^{H\times W\times C}\}_{i=1}^{n}$, rendered by alpha compositing $D = L_1 \oplus \cdots \oplus L_n$. Given a document-level instruction I_D, the reasoning stage is performed by a VLM-based reasoner $\mathcal{R}_\phi(D, I_D) \mapsto \hat{\mathcal{I}} = \{\hat{I}_i\}_{i=1}^{n}$, which predicts layer-specific instructions where each $\hat{I}_i$ either specifies an edit for layer L_i or is a `no-op` indicating that the layer should remain unchanged. The editing stage is handled by an image-generation editor $\mathcal{E}(\mathcal{L}, I_D, \hat{\mathcal{I}}) \mapsto D'$, which updates the document by applying $L'_i = \mathcal{E}(L_i, \hat{I}_i)$ if $\hat{I}_i \neq$ `no-op`, and $L'_i = L_i$ otherwise. The final edited document is then reconstructed in the original order as $D' = L'_1 \oplus \cdots \oplus L'_n$. A valid solution must satisfy *instruction compliance* (the output follows the semantics, text, and attributes of I_D), *structural fidelity* (the global layout and all non-target

content remain intact), and *layer awareness* (all and only the layers in $S^\star$ are modified). For diagnostic evaluation, the benchmark provides gold supervision in the form of $S^\star$ and $\mathcal{I}$, enabling measurement of both document-level success (instruction following and fidelity) and decision quality (correctness of layer selection and alignment). Each benchmark instance is therefore specified by five components: the rendered document D, its layer decomposition $\mathcal{L}$, the document-level instruction I_D, the gold relevant-layer set $S^\star$, and the layer-wise instructions $\mathcal{I}$.

Since current open- and closed-source[1] models do not support multi-image (multi-layer) editing interfaces, we design a practical evaluation protocol that treats each method as a *black-box* editor. Specifically, the model only consumes the rendered document D and instruction I_D, and produces an edited output D'; layer-wise inputs or edits are *not* required. Even under this simplified setting, existing models fail to reliably follow instructions, preserve layout, or render texts (Table 2), underscoring the importance and difficulty of the proposed task: no previous work can fully complete it. Finally, Table 1 summarizes the dataset statistics. We also show the distribution of layers per document and prompt lengths in Figure 6 and 7 in the Appendix.

3.2 Dataset Construction Pipeline

The dataset construction pipeline consists of three steps: data collection, document-level instruction generation, and layer-wise instruction generation, with human-in-the-loop validation for the last two steps. Alg. 1 in Appendix A.1 illustrates the overall data creation pipeline. For each generated editing instruction, we ask human annotators to check whether the editing instruction is reasonable based on the design document content. If not, we filter out this example.

Table 1: Statistics of MiLDEBench

Aspect	**Train**	**Test**
Number of design documents	17.7k	1.9k
Avg. #layers per doc	4.45	4.44
Avg. #layers needing edit per doc	1.66	1.66
Avg. len of doc-level instruction	15.56	15.53
Avg. len of layer-wise instruction	24.50	24.48

Design document collection and layer consolidation. We build our corpus from the public Crello dataset (Yamaguchi, 2021), which provides transparent-background, multi-layer *design* documents represented as $(D, \mathcal{L})$, where D is the rendered document and $\mathcal{L} = \{L_i\}_{i=1}^n$ is its layer decomposition. Crello is chosen because (i) our benchmark targets real-world design workflows with non-expert users, so we exclude datasets with synthetically generated layers (*e.g.*, Magick (Burgert et al., 2024), PrismLayers (Chen et al., 2025a)); and (ii) our focus is on scenarios where text, decorative elements, and imagery interact, so we omit multi-layer resources derived from *natural* images (*e.g.*, MuLAn (Tudosiu et al., 2024), MLCID (Huang et al., 2024)). Although ART (Pu et al., 2025) introduces a large-scale design corpus, it is not publicly available and thus excluded. To make $\mathcal{L}$ tractable, we apply a *structure-preserving consolidation* procedure $\mathcal{C}(\mathcal{L}) \mapsto \mathcal{L}'$: an MLLM (InternVL3-38B (Zhu et al., 2025)) classifies layers into *text*, *decoration*, or *image*, and non-overlapping layers within each category are merged using layout metadata while preserving z-order and alpha boundaries. This reduces $|\mathcal{L}|$ (2–50) to a semantically coherent $\mathcal{L}'$ ($|\mathcal{L}'|$ varies 1-12) without discarding content.

Document-level instruction generation. Given a consolidated design document $(D, \mathcal{L})$, we generate a document-level instruction I_D for each item. We adopt a two-stream pipeline that balances diversity and realism. (i) *Persona-based stream:* six personas $p_j \sim$ PersonaHub are sampled, and InternVL3-38B generates candidate instructions $I_D^{(j)}$ by adapting D to each persona's domain while preserving its design intent (*e.g.*, "concert poster" $\rightarrow$ "historical exhibition poster", p_j is a "historian"). (ii) *Document-based stream:* the model proposes semantically proximal domain transfers grounded in D itself (*e.g.*, "summer camp" $\rightarrow$ "winter camp"). The combined candidate pool $I_D^{(j)}$ is then ranked by clarity, specificity, and realism, with low-quality cases removed through lightweight automatic filtering and regeneration until criteria are met. Finally, a human-in-the-loop validation stage removes instructions that are infeasible, yielding the final I_D.

Layer-wise instruction generation. For each benchmark instance $(D, I_D, \mathcal{L})$, we provide a set of *layer-aligned* editing instructions $\mathcal{I} = I_i$ specifying how each relevant layer should be modified to realize the document-level intent. During document-level instruction synthesis, the InternVL3-38B is simultaneously

[1]We verified that GPT-o3 could complete the task in manual trials, but the model was discontinued before our benchmark was finalized, preventing systematic evaluation.

prompted to produce step-wise edits as a program that decomposes I_D into atomic actions (*e.g.*, "replace text 'piano concert' with 'historical exhibition'"). We then align steps to layers using a novel MLLM-based content-aware matcher to produce layer-wise instructions I_i. The matching algorithm is detailed in Appendix A.2. Finally, automatically generated instructions are filtered by rule-based validators and refined through human-in-the-loop expert review, ensuring clarity, feasibility, and faithfulness to real design workflows. The resulting edited layers $S^\star$ and aligned instructions $\mathcal{I}$ thus combine automated alignment with human refinement to provide reliable gold supervision.

4 Benchmarking with MiLDEBench

4.1 MiLDEEval

For a comprehensive assessment of our benchmark, we introduce **MiLDEEval**, which encompasses four key evaluation dimensions: instruction following, layout consistency, aesthetics, and text rendering. To holistically reflect model performance on the task, we further integrate the four perceptual criteria into a unified score, denoted as **MiLDEScore**.

Instruction Following. To assess whether the model faithfully executes an editing instruction I_D, we design a VQA-style evaluation metric. Given the document D, the target layer $S^\star$, and its layer-specific prompt $\mathcal{I}$, InternVL3-38B is prompted to generate a question–answer pair for each edited layer. Each question explicitly grounds the edit in spatial, textual, or entity-level detail (*e.g.*, *"Has the main image be changed to a museum scene?"*), with a binary answer of "yes" or "no." The instruction-following score is defined as the proportion of edits judged correct across all layers.

Layout Consistency. To evaluate structural fidelity, we measure layout consistency between original and edited documents using mask-level representations. We extract spatial masks $\mathcal{M} = \{M_i\}$ and $\mathcal{M}' = \{M'_j\}$ using Adopd Doc2Mask model (Gu et al., 2024) from the original document D and edited document D', then we design a new matching algorithm to match the two sets of spatial masks. The detailed calculation function is shown in Appendix B.1.

Aesthetics. We assess whether edits preserve or improve overall visual appeal using a frozen aesthetics predictor (*Aesthetic Predictor V2.5* (aes)). We directly utilize the score as final evaluation.

Text Rendering. We evaluate the *faithfulness* of edited text with an OCR–VQA pipeline. We evaluate the *faithfulness* of edited text with an OCR–VQA pipeline. Specifically, we first apply the Adopd Doc2BBox model (Gu et al., 2024) to detect text regions in the edited image L'_j, and then use InternVL3-38B to extract the corresponding text t'. Given the instruction I_D, we prompt the MLLM to verify whether t' satisfies the required edit, producing a score in $\{0, 0.5, 1\}$. Unlike conventional text-alignment metrics (*e.g.*, SentenceBERT (Reimers & Gurevych, 2019)), our approach does not assume a unique ground truth: multiple valid edits may satisfy I_D, and thus a judgment-based evaluation better captures instruction faithfulness.

MiLDEScore. Although the four evaluation dimensions comprehensively capture different aspects of the multi-layer design document editing task, they cannot be treated as independent objectives. For example, if an editing model fails to modify the document and simply outputs the unedited input, the *layout consistency* score would reach 100%, while *instruction following* and *text rendering* would be zero. In this case, the high layout consistency is meaningless, since it does not indicate a successful edit. To jointly model the interdependence among these factors, we introduce **MiLDEScore**, a unified metric that aggregates the four perceptual criteria into a single holistic score. Let the raw scores of *instruction following (IF)*, *layout consistency (LC)*, *text rendering (TR)*, and *aesthetics (A)* be normalized to $[0, 1]$ as:

$$\mathrm{IF}_h = \frac{\mathrm{IF}}{100}, \quad \mathrm{LC}_h = \frac{\mathrm{LC}}{100}, \quad \mathrm{TR}_h = \frac{\mathrm{TR}}{100}, \quad \mathrm{A}_h = \frac{\mathrm{A}}{10}. \tag{1}$$

We employ an instruction-following–based **sigmoid gate** to control the influence of other metrics:

$$g(\mathrm{IF}_h) = \frac{\sigma(k(\mathrm{IF}_h - \tau)) - \sigma(-k\tau)}{\sigma(k(1-\tau)) - \sigma(-k\tau)}, \quad \sigma(x) = \frac{1}{1+e^{-x}}, \tag{2}$$

Table 2: Evaluation results of different models. Layer Dec. Accuracy represents layer decision accuracy, respectively. For all scores, higher values indicate better performance. The highest score for closed-source and open-source text-to-image models are marked in red and blue respectively, and underline represents the second in open-source models. Note that for previous baselines incapable of multi-layer editing, the *layer decision accuracy* metric is not applicable.

#	Model	Instruction Following	Layout Consistency	Aesthetic	Text Rendering	MiLDEScore	Layer Dec. Accuracy
	Open-source Models						
1	Instruct-Pix2Pix (Brooks et al., 2023)	2.30	93.46	4.23	17.16	6.23	–
2	MagicBrush (Zhang et al., 2023a)	7.37	72.08	3.68	16.60	8.47	–
3	UniWorld-v1 (Lin et al., 2025)	5.75	61.59	3.91	22.04	9.15	–
4	VAREdit (Mao et al., 2025)	6.60	68.10	3.18	9.49	5.86	–
5	UltraEdit (Zhao et al., 2024)	12.41	85.31	3.54	11.39	10.35	–
6	AnyEdit (Yu et al., 2025a)	6.51	56.73	3.96	21.83	9.40	–
7	OmniGen (Xiao et al., 2025a)	3.83	85.96	3.90	19.76	7.73	–
8	Qwen-Image-Edit (Wu et al., 2025a)	10.09	74.20	4.12	24.32	12.42	–
9	Flux1-Kontext (Batifol et al., 2025)	12.49	48.32	3.94	19.31	11.58	–
10	Step1X-Edit (Liu et al., 2025)	6.56	84.09	3.98	18.70	8.84	–
11	Bagel (Deng et al., 2025)	14.23	48.59	3.54	13.49	10.80	–
	Reasoning-enhanced Models						
12	Step1X-Edit w/ Thinking	10.48	82.16	4.11	28.67	14.17	–
13	Bagel w/ Thinking	13.60	60.91	3.65	14.51	11.23	–
	Closed-source Models						
14	GPT-Image-1 (OpenAI, 2025)	25.46	36.24	4.66	39.67	25.60	–
15	Nano Banana (DeepMind, 2025)	24.04	58.42	4.52	40.32	27.10	–
	***MiLDEAgent** (Ours)*						
16	Qwen2.5VL-3B + Flux	13.29	90.15	4.32	27.52	16.10	42.90
17	Qwen2.5VL-7B + Flux	20.71	93.24	4.19	36.75	25.90	80.46

where τ defines the gate threshold and k controls the steepness. A higher τ makes the gate stricter, while a larger k sharpens the transition. The overall **MiLDEScore** is computed as:

$$\text{MiLDEScore} = w_{\text{if}}\text{IF}_h + w_{\text{tr}}\text{TR}_h + g(\text{IF}_h)\,(w_{\text{lc}}\text{LC}_h + w_{\text{a}}\text{A}_h) + w_{\text{sy}}\,g(\text{IF}_h)\,\text{IF}_h\,\text{LC}_h. \tag{3}$$

The sigmoid gate $g(\text{IF}_h)$ ensures that *layout consistency* and *aesthetics* only contribute meaningfully when the instruction-following score is sufficiently high. When the model fails to follow the editing instruction ($\text{IF}_h < \tau$), the gate value remains near zero, effectively suppressing irrelevant high LC or A scores. As IF_h increases, these terms are gradually activated, allowing models that both follow instructions and preserve layout to achieve higher overall scores. The last term $w_{\text{sy}}g(\text{IF}_h)\text{IF}_h\text{LC}_h$ captures the synergy between instruction accuracy and spatial consistency. It provides an additional reward when both metrics are simultaneously high, reflecting the natural coupling between semantic correctness and visual coherence in human judgment. More details are discussed in Appendix D.2.

Layer Decision Accuracy. In addition to metrics for edited document quality, we also incorporate another metric called layer decision accuracy. As shown in Figure 1, in many cases in our benchmark, not all layers require modification. Therefore, we additionally report the layer decision accuracy to measure whether the model can correctly identify which layers should be edited.

4.2 Evaluation and Analysis

To conduct evaluation on **MiLDEBench**, we conduct comprehensive evaluation on 13 open-source models, with 11 reasoning-free models and 2 reasoning-enhanced models, and 2 closed-source models. Note that in these experiments, we only take design document D and document-level editing instruction I_D as input, because current models cannot conduct multiple-layer editing simultaneously. Specifically, the task here is $\mathcal{E}(D, I_D) \rightarrow D'$. The primary results are presented in Table 2. Please refer to Appendix C for detailed experiment and evaluation setup.

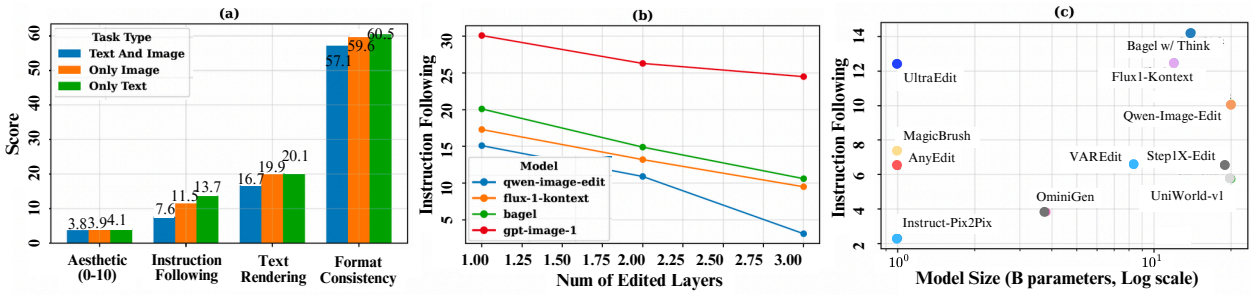

Figure 2: (a) Evaluation metrics with editing type. (b) Instruction following score with the number of edited layers. (c) Instruction following the model size.

Finding 1: Current image editing models struggle with design document editing. Our evaluation reveals that both open-source and closed-source models exhibit certain limitations in instruction following and text rendering. For open-source models (`#1-#11`), the average instruction-following accuracy is only about 10%, meaning that in nearly 90% of cases the specified edits are not correctly executed. Even the strongest closed-source baseline, GPT-Image-1 (`#14`), achieves only 25.46% instruction following accuracy, underscoring the substantial gap between current image editing capabilities and the demands of multi-layer document editing in realistic scenarios.

Finding 2: Closed-source models trade layout consistency for instruction following. Closed-source models (e.g., GPT-Image-1, Nano Banana) significantly outperform open-source counterparts in instruction following, text rendering, and aesthetics. For instance, GPT-Image-1 (`#14`) nearly doubles the instruction accuracy of the best open-source model, Bagel (`#11`) (25.46% vs. 14.23%). Similarly, Nano Banana (`#15`) leads in text rendering (40.32%) over Step1X-Edit (`#12`). However, these gains often come at the cost of layout consistency, where GPT-Image-1 achieves the lowest scores. Notably, the higher consistency scores in open-source models frequently stem from "trivial artifacts"—simply outputting the unedited document. This reveals a critical trade-off: while closed-source models follow intent more reliably, they struggle to maintain the structural fidelity essential for real-world design workflows.

Finding 3: Explicit reasoning mechanisms yield marginal gains for document editing. Integrating explicit reasoning ("w/ Thinking") into open-source editors provides limited improvements. While Step1X-Edit (`#10`) shows a modest boost in instruction accuracy (from 6.56% to 10.48%), Bagel (`#11`), conversely, shows a slight performance decline. These results suggest that current reasoning modules primarily capture textual intent but fail to ground edits within complex multi-layer structures, especially when simultaneous text and image modifications are required. This underscores the need for deep multimodal reasoning integration rather than shallow textual planning to truly advance document editing capabilities.

Finding 4: Performance degrades sharply as editing complexity and layer depth increase. Model efficacy is highly sensitive to task complexity across modalities and structure. As shown in Figure 2 (a), instruction following drops significantly when transitioning from single-modality edits (e.g., 13.7% for text-only) to combined text+image tasks (7.6%). Furthermore, Figure 2 (b) demonstrates that layer depth poses a major challenge: Bagel's accuracy falls from 20.1% (one layer) to 10.6% (three layers), a trend mirrored by even the strongest closed-source models. Finally, 2 (c) shows that larger model size does not consistently yield improvements, suggesting that the bottleneck lies in multimodal reasoning capability rather than pure parameter scaling. These findings highlight the difficulty current models face in navigating complex, multi-layered editing intents.

5 The MiLDEAgent Framework

Recognizing the reasoning inaccuracies, layout consistency issue and the fundamental problem that current image editing model cannot do multiple layer editng, we propose **MiLDEAgent**, consisting of an RL-trained reasoner and a frozen image editor. Specifically, our agent receives a design document D with multiple

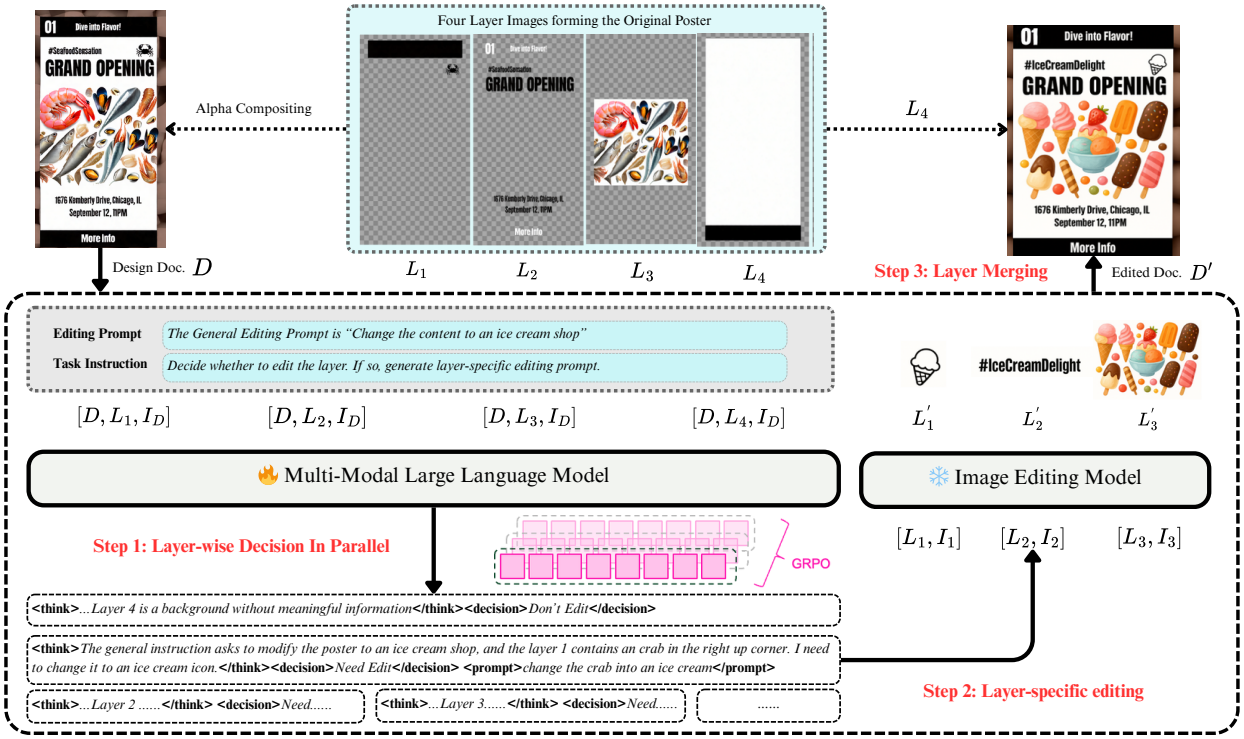

Figure 3: The illustration of MiLDEAgent.

transparent background layers $\mathcal{L}$ and a document-level instruction I_D, and then produce D' by editing *exactly* the relevant layers and re-compositing them in the original z-order. Specifically, the task here is $Agent(D, I_D, \mathcal{L}) \rightarrow (D', \mathcal{L}')$. We introduce our agent in Section 5.1 and evaluate on our benchmark, including ablation studies and human evaluation, on Section 5.2.

5.1 Reasoning-Guided Multi-Layer Document Editing

As shown in Figure 3, our **MiLDEAgent** is a two-stage framework for multi-layer document editing, where the reasoner $\mathcal{R}_\phi$ performs instruction decomposition and the editor $\mathcal{E}$ performs layer-wise editing.

Reasoning. The reasoning stage is handled by a VLM-based reasoner $\mathcal{R}_\phi$, which takes (D, L_i, I_D) as input and outputs for each layer a binary decision $y_i \in \{0, 1\}$ and, if $y_i = 1$, a *layer-conditioned prompt* I_i. To train $\mathcal{R}_\phi$, we adopt Group Relative Policy Optimization (GRPO) (Shao et al., 2024), a RL method that evaluates groups of sampled responses, computes relative advantages by normalizing their rewards, and applies a clipped KL-regularized objective. This design reduces variance in credit assignment and encourages the model to distinguish between relatively better and worse responses, which is particularly beneficial for structured reasoning tasks (see Appendix D.1 for details).

Following this paradigm, we design a task-specific per-layer reward to supervise $\mathcal{R}_\phi$. The outputs of the reasoner must follow a structured format:

$$\texttt{<think>}\ldots\texttt{</think><decision>}\ldots\texttt{</decision><prompt>}\ldots\texttt{</prompt>} \tag{4}$$

where the three segments denote hidden reasoning, the binary decision y_i, and the layer-conditioned prompt I_i, respectively. The per-layer reward $\mathcal{R}_i$ then consists of three components:

$$r_f = \mathbb{1}[\text{format is valid}], \quad r_d = \mathbb{1}[y_i = y_i^\star], \quad r_p = \text{BLEU}(I_i, I_i^\star) \in [0, 1]. \tag{5}$$

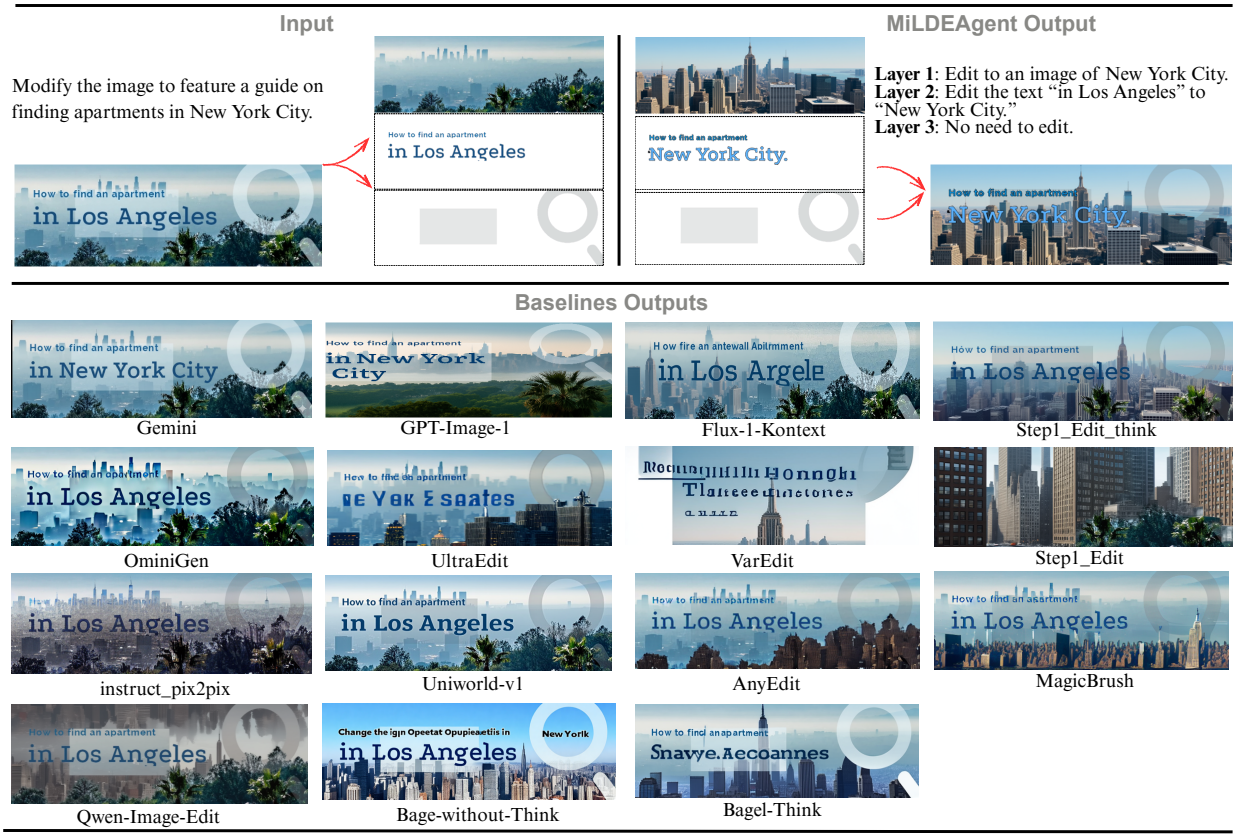

Figure 4: Qualitative comparison results between MiLDEAgent and other baselines. The input consists of one user's query and three layers, which compose the original design document. MiLDEAgent's output includes layer decisions and edited layers, which compose the final edited design document.

The final per-layer reward is defined as

$$\mathcal{R}_i = \begin{cases} (r_f + r_d + r_p)/3, & r_d = 1, \\ (r_f + r_d)/2, & r_d = 0 \ . \end{cases} \tag{6}$$

where r_f verifies syntactic correctness, r_d measures decision accuracy against the gold label $y_i^\star = \mathbb{1}[L_i \in S^\star]$, and r_p evaluates prompt quality relative to the reference instruction $I_i^\star$. The prompt reward r_p is only applied when the decision is correct ($r_d = 1$).

Editing. The editing stage uses a frozen image-generation editor $\mathcal{E}$ for stability and modularity. For each selected layer L_i ($y_i = 1$), a binary mask M_i is extracted from its alpha channel (optionally refined with region cues), and the editor updates it as $L_i' = \mathcal{E}(L_i, I_i, M_i)$. For non-selected layers ($y_i = 0$), no operation is applied and $L_i' = L_i$. Transparency is preserved by restoring the original alpha to unedited regions. Please note that we do not allow changes to geometry (e.g., text reshaping or object movement) as our task asks the model to preserve the original format. We acknowledge that in some cases, it is necessary to change the text shaping, and we leave such situations as future work. The final document is reconstructed by alpha compositing $D' = L_1' \oplus L_2' \oplus \cdots \oplus L_n'$, where $\oplus$ denotes standard alpha blending, ensuring global layout consistency while fulfilling the document-level instruction I_D.

5.2 Experimental Results

Setup. We incorporate one of the SOTA MLLM, `QwenVL2.5-3B/7B` (Bai et al., 2025) as our reasoner, and applied the GRPO algorithm to train on content editing tasks, with a frozen `Flux-1-Kontext` as editing model. The rollout number is 5 and the batch size is 512. Experiments are conducted on 8 A100 GPUs.

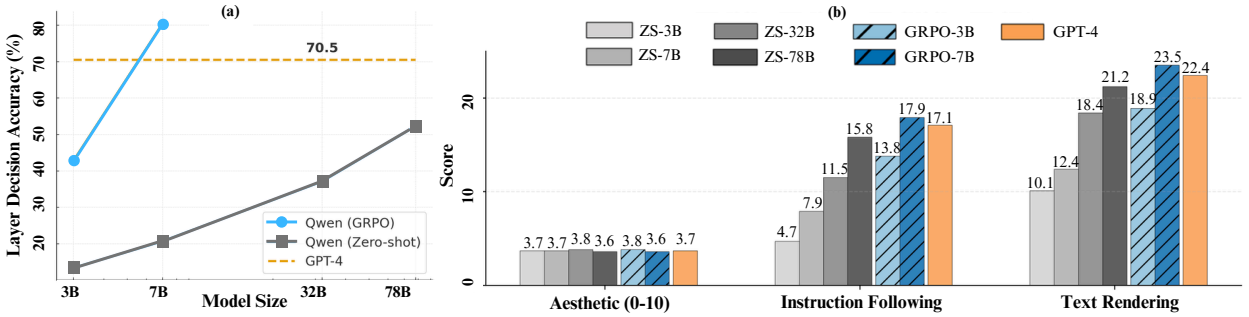

Figure 5: (a) Results of layer decision accuracy versus model sizes. (b) Evaluation metrics with different reasoning models. ZS-xB represents the reasoning models without training, while GRPO-xB represents the GRPO-trained reasoning models. We choose Flux1-Kontext as the editor.

Quantitative Results. As shown in Table 2, our proposed MiLDEAgent substantially outperforms all baselines in the content editing regime. MiLDEAgent achieves 25.9% in MiLDEScore an 82.78% improvement over the strongest open-source baseline (Bagel, 14.17%), narrowing the gap with closed-source systems (Nano Banana, 27.1%) and even surpassing GPT-Image-1 (25.6%) while preserving editability. Beyond overall editing quality, the 7B MiLDEAgent also outperforms all open-source baselines on instruction following, and maintains strong layout consistency at 93.2%, matching the best diffusion-based editors and exceeding closed-source models by over +30 points. Notably, our agent shows markedly stronger text rendering (36.8%), outperforming all open-source baselines ($\leq$ 24.3%) and approaching commercial systems (40%), which underscores the advantage of our reasoning-based design for multi-layer textual elements. Finally, MiLDEAgent achieves 80.5% layer decision accuracy, demonstrating robust layer-aware reasoning that is entirely absent from existing baselines and validating the necessity of reasoning-enhanced frameworks for this task. Taken together, these results indicate that multi-layer document editing benefits from explicit reasoning mechanisms rather than relying solely on generation or editing heuristics: MiLDEAgent consistently balances instruction fidelity, fine-grained text rendering, and layer-aware decomposition, making it the first system to robustly address multi-layer editing at scale.

Quality Analysis. As illustrated in Figure 4, the input design document consists of three layers. Our agent successfully identifies that the first layer, which contains the background image of Los Angeles, should be edited to depict New York City. In addition, the text "in Los Angeles" in the second layer is correctly modified to "New York City." The third layer, however, is purely decorative and is correctly recognized as not requiring any modification. After applying an open-source image editing model, our agent composites the edited layers with the unedited ones to form the final output. The resulting image preserves the original layout while accurately updating the relevant content, and it also retains per-layer information for future flexible modifications by users. In contrast, all other baselines fail in this task, even under single-image editing settings. For instance, Gemini only changes the textual content without modifying the background image, whereas GPT-Image-1 fails to maintain layout consistency. Other open-source baselines either fail to edit the text (e.g., OmniGen, Step1-Edit) or completely fail to perform meaningful edits (e.g., VarEdit).

Ablation 1: GRPO-trained reasoner outperforms all zero-shot models in layer decision accuracy. Reasoner is the key to MiLDEAgent, therefore, we conduct an ablation study on the RL-trained reasoner with other larger open-/closed-source MLLMs on layer decision accuracy metrics. As shown in Figure 5 (a), we observe that models equipped with a GRPO-trained reasoner consistently surpass their zero-shot counterparts across all tested scales. For instance, QwenVL2.5-7B with GRPO achieves 80.5% accuracy, compared to only 20.7% for its zero-shot variant, a nearly 4$\times$ improvement, and outperforms GPT-4 by 13.6%, highlighting that structured reinforcement-style reasoning is beneficial even at smaller scales. We further randomly select 100 samples to test the final editing. As shown in Figure 5 (b), using the GRPO-trained 7B model outperforms GPT-4 in both instruction following and text rendering, which is consistent with the layer decision accuracy results. These results underscore that reasoning-oriented training is the dominant factor for reliable layer decision making, establishing GRPO as a crucial ingredient for advancing multi-layer document editing.

Table 4: Human evaluation on **MiLDEBench** (left) and **Inter-Annotator Agreement** (right, Cohen's κ). IF, LC, Aes. TR, OQ represent instruction following, layout consistency, aesthetic, text rendering, and overall quality, respectively.

#	Model	IF	LC	Aes.	TR	OQ
Baselines						
1	Instruct-Pix2Pix	0.05	2.85	1.23	0.67	0.27
2	MagicBrush	0.35	2.27	1.07	0.59	0.28
13	Bagel w/ Thinking	0.87	2.05	1.16	0.58	0.39
15	Nano Banana	1.34	1.76	1.95	1.84	1.45
MiLDEAgent *(Ours)*						
17	Qwen2.5VL-7B + Flux	1.28	2.83	1.27	1.75	1.37

Metric	κ
IF	0.75
LC	0.71
Aes.	0.61
TR	0.72
OQ	0.69
AVG	0.70

Ablation 2: Image editing model also influence the final performance. In this experiment, we randomly select 100 samples from the content editing test set and utilize the GRPO-trained QwenVL2.5-7B model as reasoner to test different image editing models. As shown in Table 3, GPT-Image-1 consistently achieves the best overall results, with 19.7% in instruction following, 4.4% in aesthetics, and 30.6% in text rendering, outperforming the best open-source alternatives by a clear margin. Among open-source models, Qwen-Image-Edit exhibits relatively stronger instruction following and text rendering, while Bagel and Flux1-Kontext are more balanced but weaker in fidelity and reasoning. These results indicate that even with the same reasoning mechanism, the fidelity and controllability of the editing backbone strongly shape the final quality of document editing. Finally, we acknowledge that using a more powerful image editing model will improve the performance, but this will not influence the main conclusion of our findings.

Table 3: Evaluation score with different image editing models.

Model	IF	Aes.	TR
Qwen-Image-Edit	18.5	4.0	26.4
Flux-1-Kontext	17.9	3.65	23.5
Bagel	17.3	3.76	25.4
GPT-Image-1	19.7	4.37	30.6

Human Evaluation. We randomly sample 100 instances from **MiLDEBench** for human evaluation. To ensure representative comparison while controlling annotation cost, we include four baselines: Nano Banana (closed-source), Bagel w/ Thinking (reasoning-enhanced), and Instruct-Pix2Pix and MagicBrush (open-source). We evaluate the Qwen2.5VL-7B–based MiLDEAgent yielding 500 edited outputs (5 methods $\times$ 100 instances), each independently assessed by two annotators. Annotators consist of Ph.D. or master's students with expertise in multimodal learning, as well as professional designers experienced in document layout and visual composition. Following the protocol of MiLDEBench each output is rated on instruction following, layout consistency, aesthetic quality, and text rendering, together with an overall quality score. We adopt a discrete scale of $0, 1, 2, 3$ for efficiency, where 0 indicates failure and 1–3 correspond to poor, fair, and good quality, respectively. The aggregated results are reported in Table 4. Human judgments are consistent with the automatic metrics in Table 2: MiLDEAgent performs comparably to the closed-source Nano Banana and significantly outperforms open-source baselines across most dimensions. The average inter-annotator agreement (IAA) is approximately 0.7, indicating substantial agreement and supporting evaluation reliability; agreement on aesthetic quality is relatively lower due to its inherently subjective nature.

6 Conclusion

In this work, we introduced MiLDEBench, the first benchmark for reasoning-based multi-layer poster editing, together with a novel evaluation metric. Through comprehensive experiments, we demonstrated that existing methods struggle to accurately edit posters based on general simple editing prompt. To address these limitations, we proposed MiLDEAgent, leveraging a GRPO-trained reasoner for layer selection, coupled with an open-source image editor, significantly improving reasoning ability and editing quality.

References

Aesthetic score v2.5. https://github.com/discus0434/aesthetic-predictor-v2-5.

Veeramanohar Avudaiappan and Ritwik Murali. Reconstructing graphic design posters via visual decomposition and semantic layer translation. In *Proceedings of the Special Interest Group on Computer Graphics and Interactive Techniques Conference Posters*, pp. 1–3, 2025.

Shuai Bai, Keqin Chen, Xuejing Liu, Jialin Wang, Wenbin Ge, Sibo Song, Kai Dang, Peng Wang, Shijie Wang, Jun Tang, et al. Qwen2. 5-vl technical report. *arXiv preprint arXiv:2502.13923*, 2025.

Omer Bar-Tal, Dolev Ofri-Amar, Rafail Fridman, Yoni Kasten, and Tali Dekel. Text2live: Text-driven layered image and video editing. In *European conference on computer vision*, pp. 707–723. Springer, 2022.

Stephen Batifol, Andreas Blattmann, Frederic Boesel, Saksham Consul, Cyril Diagne, Tim Dockhorn, Jack English, Zion English, Patrick Esser, Sumith Kulal, et al. Flux. 1 kontext: Flow matching for in-context image generation and editing in latent space. *arXiv e-prints*, pp. arXiv–2506, 2025.

Tim Brooks, Aleksander Holynski, and Alexei A Efros. Instructpix2pix: Learning to follow image editing instructions. In *Proceedings of the IEEE/CVF conference on computer vision and pattern recognition*, pp. 18392–18402, 2023.

Ryan D Burgert, Brian L Price, Jason Kuen, Yijun Li, and Michael S Ryoo. Magick: A large-scale captioned dataset from matting generated images using chroma keying. In *Proceedings of the IEEE/CVF Conference on Computer Vision and Pattern Recognition*, pp. 22595–22604, 2024.

Junwen Chen, Heyang Jiang, Yanbin Wang, Keming Wu, Ji Li, Chao Zhang, Keiji Yanai, Dong Chen, and Yuhui Yuan. Prismlayers: Open data for high-quality multi-layer transparent image generative models. *arXiv preprint arXiv:2505.22523*, 2025a.

Kaijie Chen, Zihao Lin, Zhiyang Xu, Ying Shen, Yuguang Yao, Joy Rimchala, Jiaxin Zhang, and Lifu Huang. R2i-bench: Benchmarking reasoning-driven text-to-image generation. *arXiv preprint arXiv:2505.23493*, 2025b.

Google DeepMind. Gemini 2.5 flash (nano banana). https://aistudio.google.com/models/gemini-2-5-flash-image, 2025.

Chaorui Deng, Deyao Zhu, Kunchang Li, Chenhui Gou, Feng Li, Zeyu Wang, Shu Zhong, Weihao Yu, Xiaonan Nie, Ziang Song, Guang Shi, and Haoqi Fan. Emerging properties in unified multimodal pretraining. *arXiv preprint arXiv:2505.14683*, 2025.

Chengqi Duan, Rongyao Fang, Yuqing Wang, Kun Wang, Linjiang Huang, Xingyu Zeng, Hongsheng Li, and Xihui Liu. Got-r1: Unleashing reasoning capability of mllm for visual generation with reinforcement learning. *arXiv preprint arXiv:2505.17022*, 2025.

Weixi Feng, Wanrong Zhu, Tsu-jui Fu, Varun Jampani, Arjun Akula, Xuehai He, Sugato Basu, Xin Eric Wang, and William Yang Wang. Layoutgpt: Compositional visual planning and generation with large language models. *Advances in Neural Information Processing Systems*, 36:18225–18250, 2023.

Jiuxiang Gu, Xiangxi Shi, Jason Kuen, Lu Qi, Ruiyi Zhang, Anqi Liu, Ani Nenkova, and Tong Sun. Adopd: A large-scale document page decomposition dataset. In *The Twelfth International Conference on Learning Representations*, 2024.

Ziyu Guo, Renrui Zhang, Chengzhuo Tong, Zhizheng Zhao, Peng Gao, Hongsheng Li, and Pheng-Ann Heng. Can we generate images with cot? let's verify and reinforce image generation step by step. *arXiv preprint arXiv:2501.13926*, 2025.

Runhui Huang, Kaixin Cai, Jianhua Han, Xiaodan Liang, Renjing Pei, Guansong Lu, Songcen Xu, Wei Zhang, and Hang Xu. Layerdiff: Exploring text-guided multi-layered composable image synthesis via layer-collaborative diffusion model. In *European Conference on Computer Vision*, pp. 144–160. Springer, 2024.

Wenxuan Huang, Bohan Jia, Zijie Zhai, Shaosheng Cao, Zheyu Ye, Fei Zhao, Zhe Xu, Yao Hu, and Shaohui Lin. Vision-r1: Incentivizing reasoning capability in multimodal large language models. *arXiv preprint arXiv:2503.06749*, 2025.

Dongzhi Jiang, Ziyu Guo, Renrui Zhang, Zhuofan Zong, Hao Li, Le Zhuo, Shilin Yan, Pheng-Ann Heng, and Hongsheng Li. T2i-r1: Reinforcing image generation with collaborative semantic-level and token-level cot. *arXiv preprint arXiv:2505.00703*, 2025.

Ying Jin, Pengyang Ling, Xiaoyi Dong, Pan Zhang, Jiaqi Wang, and Dahua Lin. Reasonpix2pix: instruction reasoning dataset for advanced image editing. *arXiv preprint arXiv:2405.11190*, 2024.

Bin Lin, Zongjian Li, Xinhua Cheng, Yuwei Niu, Yang Ye, Xianyi He, Shenghai Yuan, Wangbo Yu, Shaodong Wang, Yunyang Ge, et al. Uniworld: High-resolution semantic encoders for unified visual understanding and generation. *arXiv preprint arXiv:2506.03147*, 2025.

Tsung-Yi Lin, Michael Maire, Serge Belongie, James Hays, Pietro Perona, Deva Ramanan, Piotr Dollár, and C Lawrence Zitnick. Microsoft coco: Common objects in context. In *European Conference on Computer Vision (ECCV)*, pp. 740–755. Springer, 2014.

Shiyu Liu, Yucheng Han, Peng Xing, Fukun Yin, Rui Wang, Wei Cheng, Jiaqi Liao, Yingming Wang, Honghao Fu, Chunrui Han, et al. Step1x-edit: A practical framework for general image editing. *arXiv preprint arXiv:2504.17761*, 2025.

Qingyang Mao, Qi Cai, Yehao Li, Yingwei Pan, Mingyue Cheng, Ting Yao, Qi Liu, and Tao Mei. Visual autoregressive modeling for instruction-guided image editing. *arXiv preprint arXiv:2508.15772*, 2025.

Hui Nie, Zhao Zhang, Yutao Cheng, Maoke Yang, Gonglei Shi, Qingsong Xie, Jie Shao, and Xinglong Wu. Decomposition of graphic design with unified multimodal model. In *Forty-second International Conference on Machine Learning*, 2025.

OpenAI. Gpt-image-1 api. OpenAI Developer Documentation, 2025. URL `https://platform.openai.com/docs/guides/image-generation?image-generation-model=gpt-image-1`. Accessed: 2025-08-29.

Kaihang Pan, Yang Wu, Wendong Bu, Kai Shen, Juncheng Li, Yingting Wang, Yunfei Li, Siliang Tang, Jun Xiao, Fei Wu, et al. Unlocking aha moments via reinforcement learning: Advancing collaborative visual comprehension and generation. *arXiv preprint arXiv:2506.01480*, 2025.

Yifan Pu, Yiming Zhao, Zhicong Tang, Ruihong Yin, Haoxing Ye, Yuhui Yuan, Dong Chen, Jianmin Bao, Sirui Zhang, Yanbin Wang, et al. Art: Anonymous region transformer for variable multi-layer transparent image generation. In *Proceedings of the Computer Vision and Pattern Recognition Conference*, pp. 7952–7962, 2025.

Nils Reimers and Iryna Gurevych. Sentence-bert: Sentence embeddings using siamese bert-networks. In *Conference on Empirical Methods in Natural Language Processing*, 2019. URL `https://api.semanticscholar.org/CorpusID:201646309`.

Christoph Schuhmann, Romain Beaumont, Richard Vencu, Cade Gordon, Ross Wightman, Mehdi Cherti, Theo Coombes, Aditya Katta, Clayton Mullis, Mitchell Wortsman, Patrick Schramowski, Sascha Kundurthy, Katherine Crowson, Ludwig Schmidt, Romain Kaczmarczyk, and Jenia Jitsev. Laion-5b: An open large-scale dataset for training next generation image-text models. In *Advances in Neural Information Processing Systems (NeurIPS) Datasets and Benchmarks Track*, 2022.

Zhihong Shao, Peiyi Wang, Qihao Zhu, Runxin Xu, Junxiao Song, Xiao Bi, Haowei Zhang, Mingchuan Zhang, YK Li, Yang Wu, et al. Deepseekmath: Pushing the limits of mathematical reasoning in open language models. *arXiv preprint arXiv:2402.03300*, 2024.

Kaiyue Sun, Rongyao Fang, Chengqi Duan, Xian Liu, and Xihui Liu. T2i-reasonbench: Benchmarking reasoning-informed text-to-image generation. *arXiv preprint arXiv:2508.17472*, 2025.

Manan Suri, Puneet Mathur, Franck Dernoncourt, Rajiv Jain, Vlad I Morariu, Ramit Sawhney, Preslav Nakov, and Dinesh Manocha. Docedit-v2: Document structure editing via multimodal llm grounding. In *Proceedings of the 2024 Conference on Empirical Methods in Natural Language Processing*, pp. 15485–15505, 2024.

Tomoyuki Suzuki, Kang-Jun Liu, Naoto Inoue, and Kota Yamaguchi. Layerd: Decomposing raster graphic designs into layers. In *Proceedings of the IEEE/CVF International Conference on Computer Vision*, pp. 17783–17792, 2025.

Petru-Daniel Tudosiu, Yongxin Yang, Shifeng Zhang, Fei Chen, Steven McDonagh, Gerasimos Lampouras, Ignacio Iacobacci, and Sarah Parisot. Mulan: A multi layer annotated dataset for controllable text-to-image generation. In *Proceedings of the IEEE/CVF Conference on Computer Vision and Pattern Recognition*, pp. 22413–22422, 2024.

Chenfei Wu, Jiahao Li, Jingren Zhou, Junyang Lin, Kaiyuan Gao, Kun Yan, Sheng-ming Yin, Shuai Bai, Xiao Xu, Yilei Chen, et al. Qwen-image technical report. *arXiv preprint arXiv:2508.02324*, 2025a.

Mingrui Wu, Lu Wang, Pu Zhao, Fangkai Yang, Jianjin Zhang, Jianfeng Liu, Yuefeng Zhan, Weihao Han, Hao Sun, Jiayi Ji, et al. Reprompt: Reasoning-augmented reprompting for text-to-image generation via reinforcement learning. *arXiv preprint arXiv:2505.17540*, 2025b.

Shitao Xiao, Yueze Wang, Junjie Zhou, Huaying Yuan, Xingrun Xing, Ruiran Yan, Chaofan Li, Shuting Wang, Tiejun Huang, and Zheng Liu. Omnigen: Unified image generation. In *Proceedings of the Computer Vision and Pattern Recognition Conference*, pp. 13294–13304, 2025a.

Yicheng Xiao, Lin Song, Yukang Chen, Yingmin Luo, Yuxin Chen, Yukang Gan, Wei Huang, Xiu Li, Xiaojuan Qi, and Ying Shan. Mindomni: Unleashing reasoning generation in vision language models with rgpo. *arXiv preprint arXiv:2505.13031*, 2025b.

Kota Yamaguchi. Canvasvae: Learning to generate vector graphic documents. *ICCV*, 2021.

Shengming Yin, Zekai Zhang, Zecheng Tang, et al. Qwen-image-layered: Towards inherent editability via layer decomposition. *arXiv preprint arXiv:2512.15603*, 2025.

Qifan Yu, Wei Chow, Zhongqi Yue, Kaihang Pan, Yang Wu, Xiaoyang Wan, Juncheng Li, Siliang Tang, Hanwang Zhang, and Yueting Zhuang. Anyedit: Mastering unified high-quality image editing for any idea. In *Proceedings of the Computer Vision and Pattern Recognition Conference*, pp. 26125–26135, 2025a.

Qiying Yu, Zheng Zhang, Ruofei Zhu, Yufeng Yuan, Xiaochen Zuo, Yu Yue, Weinan Dai, Tiantian Fan, Gaohong Liu, Lingjun Liu, et al. Dapo: An open-source llm reinforcement learning system at scale. *arXiv preprint arXiv:2503.14476*, 2025b.

Ziyun Zeng, Junhao Zhang, Wei Li, and Mike Zheng Shou. Draw-in-mind: Learning precise image editing via chain-of-thought imagination. *arXiv preprint arXiv:2509.01986*, 2025.

Dong Zhang, Lingfeng He, Rui Yan, Fei Shen, and Jinhui Tang. R-genie: Reasoning-guided generative image editing. *arXiv preprint arXiv:2505.17768*, 2025a.

Kai Zhang, Lingbo Mo, Wenhu Chen, Huan Sun, and Yu Su. Magicbrush: A manually annotated dataset for instruction-guided image editing. *Advances in Neural Information Processing Systems*, 36:31428–31449, 2023a.

Xinyang Zhang, Wentian Zhao, Xin Lu, and Jeff Chien. Text2layer: Layered image generation using latent diffusion model. *arXiv preprint arXiv:2307.09781*, 2023b.

Yu Zhang, Yunqi Li, Yifan Yang, Rui Wang, Yuqing Yang, Dai Qi, Jianmin Bao, Dongdong Chen, Chong Luo, and Lili Qiu. Reasongen-r1: Cot for autoregressive image generation models through sft and rl. *arXiv preprint arXiv:2505.24875*, 2025b.

Zechuan Zhang, Ji Xie, Yu Lu, Zongxin Yang, and Yi Yang. In-context edit: Enabling instructional image editing with in-context generation in large scale diffusion transformer. *arXiv preprint arXiv:2504.20690*, 2025c.

Haozhe Zhao, Xiaojian Shawn Ma, Liang Chen, Shuzheng Si, Rujie Wu, Kaikai An, Peiyu Yu, Minjia Zhang, Qing Li, and Baobao Chang. Ultraedit: Instruction-based fine-grained image editing at scale. *Advances in Neural Information Processing Systems*, 37:3058–3093, 2024.

Jinguo Zhu, Weiyun Wang, Zhe Chen, Zhaoyang Liu, Shenglong Ye, Lixin Gu, Hao Tian, Yuchen Duan, Weijie Su, Jie Shao, et al. Internvl3: Exploring advanced training and test-time recipes for open-source multimodal models. *arXiv preprint arXiv:2504.10479*, 2025.

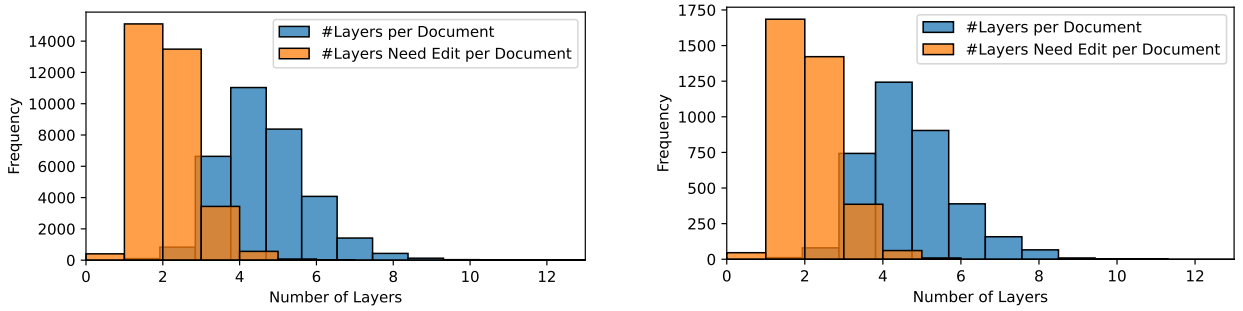

(a) Train set #layer distribution.

(b) Test set #layer distribution.

Figure 6: Distributions of the total number of layers per document and the number of layers requiring edits per document in the MiLDEBench.

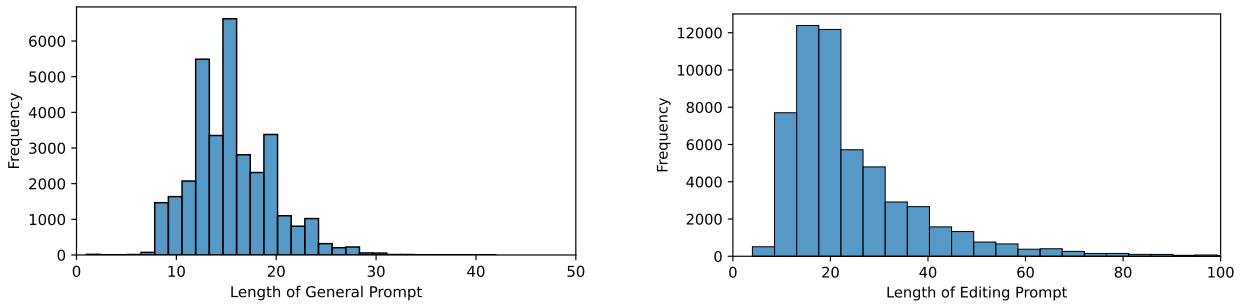

(a) Distribution of general prompt length.

(b) Distribution of editing prompt length.

Figure 7: Distributions of general prompt lengths and the editing prompt lengths in the MiLDEBench.

A MiLDEBench

A.1 Data Generation Pipeline

Algorithm 1: Data Construction Pipeline

Input : Design document D with layers $\mathcal{L}$

Output : Validated document-level instruction I_D, layer-wise instructions $\mathcal{I} = \{I_i\}$, edited layers $S^\star$

Part A: Document-level Instruction Generation

1. Generate candidate instructions $\{I_D^j\}$ from D via personas $p_j \sim$ PersonaHub;
2. Rank and filter $\{I_D^j\}$ by clarity, realism, and consistency;
3. Human validation $\Rightarrow$ finalize I_D.

Part B: Layer-wise Instruction Generation

1. Decompose I_D into step-wise edits $\mathcal{A} = \{a_j\}$;
2. Match each a_j to candidate layers $L_k \in \mathcal{L}$ using content-aware alignment;
3. Form preliminary instructions I_k and filter by clarity, feasibility, and consistency;
4. Human validation $\Rightarrow$ finalize $\mathcal{I}$ and relevant-layer set $S^\star$.

A.2 Layer-wise Instruction Generation

In this section, we describe the matcher used to align step-wise editing prompts with document layers. Given a set of step-wise prompts $\mathcal{I}_k$ and the layer set S_j with known types (textual or visual), we first classify each prompt $\mathcal{I}_k$ using InternVL3-38B into either a *text-editing* or an *image-editing* category. A prompt is

considered eligible only for layers of the corresponding type (i.e., text prompts for textual layers, image prompts for visual layers). Within each category, we process prompts sequentially: for each $\mathcal{I}_k$, we traverse the candidate layers in z-order and query InternVL3-38B to assess whether $\mathcal{I}_k$ semantically applies to S_j. Upon a positive match, $\mathcal{I}_k$ is assigned to S_j, and the procedure advances to the next prompt. This iterative matching continues until all prompts have been assigned or no valid layer remains.

B MiLDEEval

B.1 Layout Consistency

To evaluate structural fidelity, we measure layout consistency between original and edited documents using mask-level representations. We extract spatial masks $\mathcal{M} = \{M_i\}$ and $\mathcal{M}' = \{M'_j\}$ using Adopd Doc2Mask model (Gu et al., 2024) from the original document D and edited document D', then we design a new matching algorithm to match the two sets of spatial masks. For matched pairs, we assess position consistency (normalized centroid displacement), shape consistency (IoU), and area consistency (size ratio). Unmatched layers incur area-proportional penalties, with deleted layers penalized more heavily than newly created ones. The final score combines matching rate, average consistency scores, and penalty deductions with empirically tuned weights, providing a comprehensive measure of layout preservation robust to structural variations.

To assess the **structural fidelity** requirement—specifically whether the edited document D' preserves the spatial arrangement and geometric relationships of elements—we introduce a comprehensive layout consistency metric that operates on mask-level representations of document layers. Given the inherent challenges of multi-layer editing where the number of layers may change ($|\mathcal{L}'| \neq |\mathcal{L}|$) and layer correspondences may be disrupted due to editing operations, our evaluation framework employs a principled matching strategy followed by multi-dimensional consistency assessment.

Mask Extraction and Matching. For both the original document D and edited document D', we extract layer-wise masks $\mathcal{M} = \{M_i\}_{i=1}^{|\mathcal{L}|}$ and $\mathcal{M}' = \{M'_j\}_{j=1}^{|\mathcal{L}'|}$ respectively using Adopd Doc2Mask model Gu et al. (2024), where each mask $M_i \in [0,1]^{H \times W}$ represents the spatial footprint of layer L_i. To establish correspondences between original and edited layers, we formulate mask matching as a bipartite graph optimization problem: we compute a pairwise IoU similarity matrix $\mathbf{S} \in \mathbb{R}^{|\mathcal{L}| \times |\mathcal{L}'|}$ where $S_{ij} = \text{IoU}(M_i, M'_j)$, then apply the Hungarian algorithm to find the optimal matching $\mathcal{P}^* = \arg\max_{\mathcal{P}} \sum_{(i,j)\in\mathcal{P}} S_{ij}$ subject to IoU threshold filtering ($S_{ij} \geq \tau_{\text{IoU}}$).

Multi-Dimensional Consistency Assessment. For each matched pair $(M_i, M'_j) \in \mathcal{P}^*$, we evaluate three complementary aspects of layout preservation: (1) **Position consistency** measures centroid displacement normalized by image diagonal: $c_{\text{pos}}(M_i, M'_j) = 1 - \frac{\|\text{centroid}(M_i) - \text{centroid}(M'_j)\|_2}{\sqrt{H^2+W^2}}$; (2) **Shape consistency** directly uses the IoU between masks: $c_{\text{shape}}(M_i, M'_j) = \text{IoU}(M_i, M'_j)$; (3) **Area consistency** computes the ratio of smaller to larger mask areas: $c_{\text{area}}(M_i, M'_j) = \frac{\min(\text{area}(M_i), \text{area}(M'_j))}{\max(\text{area}(M_i), \text{area}(M'_j))}$.

Unmatched Layer Penalty. To account for layers that appear or disappear during editing, we introduce a penalty mechanism that distinguishes between disappeared layers (present in $\mathcal{L}$ but unmatched in $\mathcal{L}'$) and newly created layers (present in $\mathcal{L}'$ but unmatched in $\mathcal{L}$). The penalty for each unmatched layer is proportional to its normalized area, with disappeared layers receiving full penalty and new layers receiving a reduced penalty (coefficient 0.7) to reflect that layer creation may be intentional: $p_{\text{disappeared}} = \sum_{i \in \mathcal{U}_{\text{orig}}} \text{area}(M_i)$ and $p_{\text{new}} = 0.7 \sum_{j \in \mathcal{U}_{\text{edit}}} \text{area}(M'_j)$, where $\mathcal{U}_{\text{orig}}$ and $\mathcal{U}_{\text{edit}}$ denote unmatched layer indices.

Final Score Computation. The overall layout consistency score aggregates matched-layer performance with unmatched-layer penalties:

$$\begin{aligned}\text{LayoutConsistency} = \max\Big(0, \omega_{\text{match}} \cdot r_{\text{match}} + \omega_{\text{pos}} \cdot \bar{c}_{\text{pos}} + \omega_{\text{shape}} \cdot \bar{c}_{\text{shape}} \\ + \omega_{\text{area}} \cdot \bar{c}_{\text{area}} - \omega_{\text{penalty}} \cdot (p_{\text{disappeared}} + p_{\text{new}})\Big),\end{aligned} \tag{7}$$

Table 5: Introduce of each baseline model. Rea.-En. represents whether the model is reasoning-enhanced.

Model	Size	Type	Rea.-En.
Instruct-Pix2Pix Brooks et al. (2023)	1B	Diffusion	✗
MagicBrush Zhang et al. (2023a)	1B	Diffusion	✗
UniWorld-v1 Lin et al. (2025)	20B	Diffusion	✗
ICEdit Zhang et al. (2025c)	12B	Diffusion	✗
UltraEdit Zhao et al. (2024)	1B	Diffusion	✗
AnyEdit Yu et al. (2025a)	1B	Diffusion	✗
OmniGen Xiao et al. (2025a)	3.8B	Diffusion	✗
Step1X-Edit Liu et al. (2025)	19B	Diffusion	✗
Qwen-Image-Edit Wu et al. (2025a)	20B	Diffusion	✗
Flux1-Kontext Batifol et al. (2025)	12B	Diffusion	✗
Bagel w/o Think Deng et al. (2025)	14B	Diffusion	✗
Bagel w/ Think Deng et al. (2025)	14B	Diffusion	✓
VAREdit Mao et al. (2025)	8.4B	AR	✗
DIM-Edit Zeng et al. (2025)	4.6B	Diffusion	✗

where $r_{\text{match}} = \frac{|\mathcal{P}^*|}{\max(|\mathcal{L}|,|\mathcal{L}'|)}$ is the matching rate, $\bar{c}_\cdot$ denotes average consistency scores across matched pairs, and $\{\omega_\cdot\}$ are empirically set weights (0.25, 0.2, 0.2, 0.2, 0.15 respectively). This metric provides a comprehensive assessment of layout preservation that is robust to layer count variations and sensitive to both geometric distortions and structural changes.

C Experiments

C.1 Baseline Models

Baseline Open-source Models We evaluate on 13 open-source models covering auto regressive and diffusion-based framework. The model size ranges from 1B to 20B. The details of each model are shown in Table 5.

C.2 MiLDEScore

In Table 2, we set $\tau = 0.3$, $k = 10.0$, $w_{if} = 0.30$, $w_{lc} = 0.30$, $w_{tr} = 0.30$, $w_a = 0.10$, and $w_{sy} = 0.15$. We discuss the reason we chose these in Section D.2 and D.3.

D MiLDEAgent

D.1 Preliminary of GRPO Algorithm

Group Relative Policy Optimization (GRPO) (Shao et al., 2024) has been proved to be helpful for improving reasoning capabilities for LLM (Shao et al., 2024), Multi-modal understanding (Huang et al., 2025) and even image generation (Zhang et al., 2025b; Jiang et al., 2025). GRPO computes advantages from a group of responses. Given each question-anwer pair (q, a), old policy $\pi_{\theta_{\text{old}}}$ randomly samples G responses, denoted as $\{o_i\}_{i=1}^G$. Each response o_i is then fed into a reward model to obtain a reward R_i. Then, the advantage of the i-th response is obtained by normalizing the rewards of the group:

$$A_i = \frac{\mathcal{R} - \text{mean}(\{\mathcal{R}_i\}_{i=1}^G)}{\text{std}(\{\mathcal{R}_i\}_{i=1}^G)} \tag{8}$$

GRPO applies a clipped objective similar to PPO with a KL penalty term:

$$\mathcal{J}_{\text{GRPO}}(\theta) = \mathbb{E}_{(q,a)\sim\mathcal{D},\{o_i\}_{i=1}^{G}\sim\pi_{\theta_{\text{old}}}(\cdot|q)}\Bigg[\frac{1}{\sum_{i=1}^{G}|o_i|} \sum_{i=1}^{G}\sum_{t=1}^{|o_i|}\Big(\min\big(r_{i,t}(\theta)\hat{A}_i, \text{clip}(r_{i,t}(\theta), 1-\varepsilon, 1+\varepsilon)\hat{A}_i\big) - \beta D_{\text{KL}}(\pi_\theta \,\|\, \pi_{\text{ref}})\Big)\Bigg] \tag{9}$$

where $r_{i,t}(\theta)$ is the important weight for each token t:

$$r_{i,j}(\theta) = \frac{\pi_\theta\left(o_{i,j} \mid q, o_{i,<j}\right)}{\pi_{\theta_{\text{old}}}\left(o_{i,t} \mid q, o_{i,<j}\right)}. \tag{10}$$

Usually, in the reasoning task with only textual output, the model is asked to generate responses following a structured format. The total rewards consist of two rule-based rewards: (1) format reward and (2) the evaluation metrics of the specific downstream task.

D.2 More Details in MiLDEScore

Motivation and Rescaling. The motivation to design the MiLDEScore is to find a comprehensive metric considering all aspects in design document editing that can overall assess the quality of the edited document. Another reason is that we should not consider each criteria separately. For example, one model may have very high layout consistency score but low instruction following score. This means that the model fails to edit the document or directly return the original document to users. In this way, a high layout consistency score is meaningless. In order to aggregate the four aspects together, we need to first scale them into the same scope. According to the Aesthetic model (aes), the scope is ranging from 1 to 10, while the other three aspects ranging from 1 to 100. Therefore, we rescale them into the same scope by dividing aesthetic score by 10 and dividing other three scores by 100.

Other Baselines. There exist multiple ways to aggregate the four metrics into an overall score. We compare our proposed method with four representative baselines: (1) **DW_sum (Direct Weighted Sum)**, (2) **GeoMean (Geometric Mean Aggregation)**, and (3) **HCoreSup (Harmonic Core–Support Aggregation)**. Each baseline captures different assumptions about metric interactions.

(1) Direct Weighted Sum (DW_sum). The most straightforward way is a linear weighted combination of the normalized scores:

$$S_{\text{DW}} = w_{if} \cdot IF_h + w_{tr} \cdot TR_h + w_{lc} \cdot LC_h + w_a \cdot A_h.$$

This method assumes each metric contributes independently and linearly. Although simple and smooth, it tends to overestimate models that exhibit high layout consistency but poor instruction following, failing to penalize unedited outputs.

(2) Geometric Mean (GeoMean). The geometric mean combines all criteria multiplicatively:

$$S_{\text{GM}} = \Big((IF_h)^{w_{if}} \cdot (TR_h)^{w_{tr}} \cdot (LC_h)^{w_{lc}} \cdot (A_h)^{w_a}\Big)^{1/\sum w},$$

which enforces that any low-dimensional score (e.g., a very low IF_h) will significantly lower the final score. This method penalizes unbalanced models but may underestimate systems that excel in one dimension while being average in others, leading to overly conservative evaluation.

(3) Harmonic Core–Support (HCoreSup). We divide metrics into "core" (*instruction following, text rendering*) and "support" (*layout consistency, aesthetics*) groups:

$$S_{\text{HC}} = \frac{2 \cdot S_{\text{core}} \cdot S_{\text{sup}}}{S_{\text{core}} + S_{\text{sup}}}, \quad S_{\text{core}} = \frac{w_{if} \cdot IF_h + w_{tr} \cdot TR_h}{w_{if} + w_{tr}}, \quad S_{\text{sup}} = \frac{w_{lc} \cdot LC_h + w_a \cdot A_h}{w_{lc} + w_a}.$$

This harmonic mean encourages balanced performance between content correctness and visual consistency, while still allowing partial compensation between the two groups.

Table 6: Ablation study on weight parameters and comparison of different scoring functions. All configurations satisfy $w_{if} + w_{lc} + w_{tr} + w_a = 1$. For MiLDEScore, the synergy weight w_{sy} is fixed at 0.15 unless otherwise noted. ρ denotes Spearman correlation with human evaluation. DW_sum, GeoMean, and HCoreSup do not utilize the synergy term.

Configuration	w_{if}	w_{lc}	w_{tr}	w_a	w_{sy}	**Spearman ρ**			
						MiLDEScore	DW_sum	GeoMean	HCoreSup
Ours (Optimal)	**0.30**	**0.30**	**0.30**	**0.10**	**0.15**	**0.88**	0.58	0.61	0.79
Varying Primary Weights									
IF Dominant (High)	0.45	0.25	0.20	0.10	0.15	0.82	0.61	**0.64**	0.80
IF Dominant (Mid)	0.40	0.25	0.25	0.10	0.15	0.85	**0.62**	0.63	**0.81**
LC Dominant (High)	0.25	0.45	0.20	0.10	0.15	0.81	0.43	0.48	0.70
LC Dominant (Mid)	0.25	0.40	0.25	0.10	0.15	0.84	0.47	0.51	0.72
TR Dominant (High)	0.20	0.25	0.45	0.10	0.15	0.79	0.49	0.53	0.71
TR Dominant (Mid)	0.25	0.25	0.40	0.10	0.15	0.83	0.52	0.55	0.74
A Dominant	0.25	0.25	0.25	0.25	0.15	0.76	0.41	0.46	0.65
Equal Weights	0.25	0.25	0.25	0.25	–	0.76	0.45	0.52	0.71
Varying Synergy Weight (MiLDEScore only)									
No Synergy	0.30	0.30	0.30	0.10	0.00	0.813	–	–	–
Low Synergy	0.30	0.30	0.30	0.10	0.05	0.842	–	–	–
High Synergy	0.30	0.30	0.30	0.10	0.25	0.856	–	–	–
Very High Synergy	0.30	0.30	0.30	0.10	0.30	0.831	–	–	–

As is shown in this table, our sigmoid-gated synergistic method achieves the highest consistency with human ratings, showing that incorporating soft gating and interaction terms better captures subjective quality assessment.

D.3 Ablation Study on Weight Parameters

To validate the effectiveness of our proposed evaluation metric and determine the optimal weight configuration, we conduct comprehensive ablation studies on the weight parameters. Our evaluation score is formulated as:

$$\text{Score} = w_{if} \cdot \hat{IF} + w_{tr} \cdot \hat{TR} + g \cdot (w_{lc} \cdot \hat{LC} + w_a \cdot \hat{A}) + w_{sy} \cdot g \cdot \hat{IF} \cdot \hat{LC} \tag{11}$$

where $\hat{IF}$, $\hat{LC}$, $\hat{TR}$, and $\hat{A}$ denote the normalized scores for Instruction Following, Local Consistency, Text Rendering, and Aesthetics, respectively. The gating function $g = \sigma(k(\hat{IF} - \tau))$ modulates the contribution of consistency and aesthetics based on instruction following performance, with $\tau = 0.3$ and $k = 10.0$. The synergy term $w_{sy} \cdot g \cdot \hat{IF} \cdot \hat{LC}$ captures the multiplicative interaction between instruction following and local consistency.

Experimental Setup. We systematically evaluate different weight configurations while satisfying the constraint $w_{if} + w_{lc} + w_{tr} + w_a = 1$. To assess the alignment between our automatic metric and human judgment, we compute the Spearman rank correlation coefficient (ρ) between the scores produced by each configuration and human evaluation scores collected from expert annotators.

Results and Analysis. As shown in Table 6, our optimal configuration ($w_{if} = 0.30$, $w_{lc} = 0.30$, $w_{tr} = 0.30$, $w_a = 0.10$, $w_{sy} = 0.15$) achieves the highest Spearman correlation of $\rho = 0.908$ with human evaluation, significantly outperforming alternative configurations. We analyze the impact of each design choice:

(1) Balanced vs. Dominant Weights. Configurations that heavily favor a single dimension (IF Dominant, LC Dominant, or TR Dominant with weights of 0.45) yield substantially lower correlations ($\rho = 0.650$), indicating that no single metric alone captures the multifaceted nature of image editing quality. Similarly, the Equal Weights configuration ($w_{if} = w_{lc} = w_{tr} = w_a = 0.25$) achieves only $\rho = 0.671$, suggesting that treating aesthetics equally with other dimensions does not align well with human preferences.

(2) Role of the Synergy Term. The synergy term proves crucial for capturing the interaction between instruction following and local consistency. Removing this term entirely (No Synergy, $w_{sy} = 0$) reduces the correlation to $\rho = 0.692$, while excessive synergy weighting (High Synergy, $w_{sy} = 0.30$) yields a similar degradation ($\rho = 0.692$). This demonstrates that moderate synergy ($w_{sy} = 0.15$) effectively models how human evaluators reward edits that simultaneously follow instructions accurately and maintain visual coherence.

(3) Comparison with Alternative Scoring Functions. We further compare MiLDEScore against three baseline aggregation methods: Direct Weighted Sum (DW_sum), Geometric Mean (GeoMean), and Harmonic Core-Support (HCoreSup). As shown in Table 6, MiLDEScore consistently outperforms all baselines across different weight configurations. Under the optimal setting, MiLDEScore achieves $\rho = 0.88$, substantially surpassing HCoreSup ($\rho = 0.79$), GeoMean ($\rho = 0.61$), and DW_sum ($\rho = 0.58$).

The performance gap stems from two key innovations in MiLDEScore: (i) the *adaptive gating mechanism* that dynamically modulates the contribution of visual quality metrics based on instruction following performance, preventing inflated scores for models that preserve content without executing the requested edit; and (ii) the *synergy term* that explicitly captures the positive interaction between instruction following and local consistency, which none of the baselines can model. Notably, even the best-performing baseline configurations (IF Dominant Mid for DW_sum and HCoreSup, IF Dominant High for GeoMean) achieve at most $\rho = 0.81$, still significantly below our optimal MiLDEScore. This consistent advantage across all configurations demonstrates that the architectural design of MiLDEScore, rather than parameter tuning alone, accounts for its superior alignment with human judgment.

E Failure Cases

Failure Cases. Our agent still exhibits certain failure modes. First, as layer decisions are made independently, multiple layers may occasionally be edited simultaneously, resulting in unintended overlaps or visual conflicts. Second, even with high-layer decision accuracy (e.g., the 7B model), The overall instruction-following score can remain low due to (i) ambiguous or underspecified layer-wise editing prompts, and (ii) the inherent limitations of the underlying image editing model. A potential solution is to integrate a self-checking mechanism that verifies the merged output and re-invokes editing when inconsistencies are detected. One example is shown in Figure 8. Our agent successfully predicts whether the layer should be edited. However, the merged document shows overlapped text and main image. This can be partially solved by self-checking mechanism in future. However, adding a self-checking mechanism is not the main story of our paper; therefore, we leave this part as our future plan.

F More Cases

We show more cases from Figure 8 to 10.

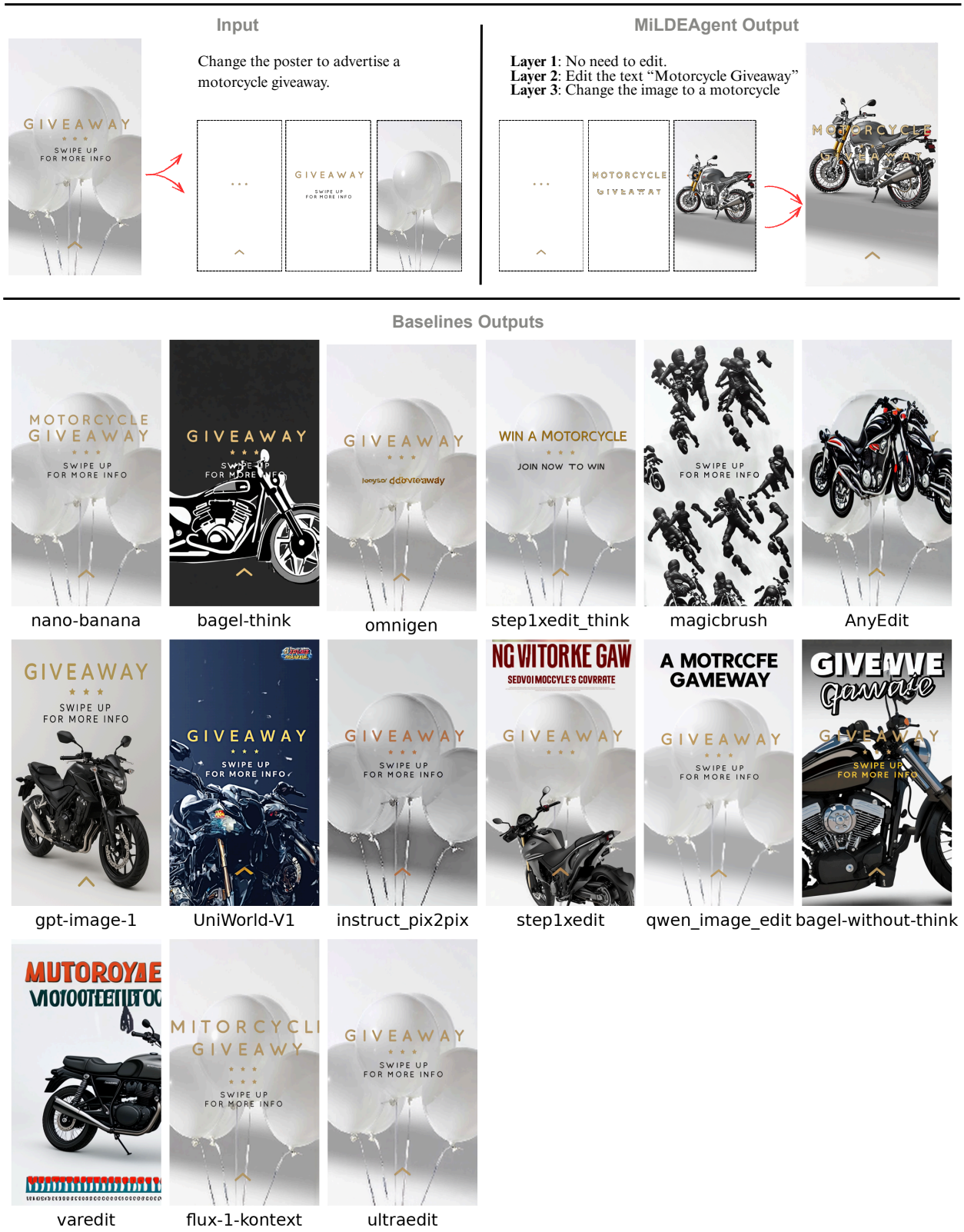

Figure 8: More examples 1.

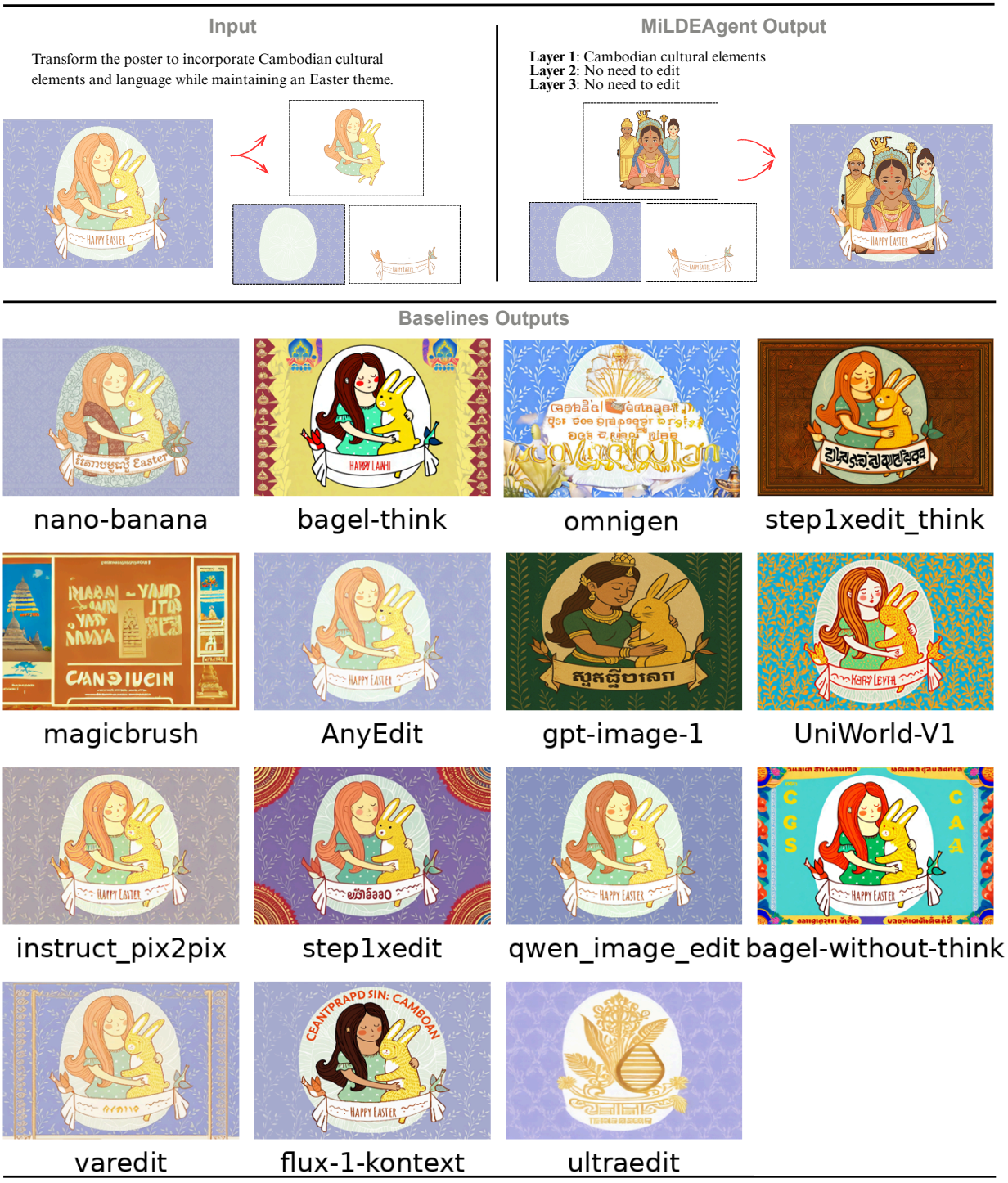

Figure 9: More examples 2.

Figure 10: More examples 3.